


Usefulness of zebrafish larvae to evaluate drug-induced functional and morphological renal tubular alterations

Rita Gorgulho¹ · Raquel Jacinto¹ · Susana S. Lopes¹ · Sofia A. Pereira¹ · Erin M. Tranfield² · Gabriel G. Martins^{2,3} · Emilio J. Gualda² · Rico J. E. Derks⁴ · Ana C. Correia² · Evelyne Steenvoorden⁴ · Petra Pintado¹ · Oleg A. Mayboroda⁴ · Emilia C. Monteiro¹ · Judit Morello¹ 

Received: 30 March 2017 / Accepted: 11 September 2017 / Published online: 20 September 2017
© Springer-Verlag GmbH Germany 2017

Abstract Prediction and management of drug-induced renal injury (DIRI) rely on the knowledge of the mechanisms of drug insult and on the availability of appropriate animal models to explore it. Zebrafish (*Danio rerio*) offers unique advantages for assessing DIRI because the larval pronephric kidney has a high homology with its human counterpart and it is fully mature at 3.5 days post-fertilization. Herein, we aimed to evaluate the usefulness of zebrafish larvae as a model of renal tubular toxicity through a comprehensive analysis of the renal alterations induced by the lethal concentrations for 10% of the larvae for gentamicin, paracetamol and tenofovir. We evaluated drug metabolic profile by mass spectrometry, renal function with the inulin clearance assay, the 3D morphology of the proximal convoluted tubule by two-photon microscopy and the ultrastructure of proximal

convoluted tubule mitochondria by transmission electron microscopy. Paracetamol was metabolized by conjugation and oxidation with further detoxification with glutathione. Renal clearance was reduced with gentamicin and paracetamol. Proximal tubules were enlarged with paracetamol and tenofovir. All drugs induced mitochondrial alterations including dysmorphic shapes (“donuts”, “pancakes” and “rods”), mitochondrial swelling, cristae disruption and/or loss of matrix granules. These results are in agreement with the tubular effects of gentamicin, paracetamol and tenofovir in man and demonstrate that zebrafish larvae might be a good model to assess functional and structural damage associated with DIRI.

Keywords Nephrotoxicity · Proximal tubule · Mitochondria · Renal clearance · Zebrafish

Rita Gorgulho and Raquel Jacinto contributed equally to the study.

Electronic supplementary material The online version of this article (doi:10.1007/s00204-017-2063-1) contains supplementary material, which is available to authorized users.

✉ Judit Morello
judit.morello@nms.unl.pt

- ¹ Chronic Diseases Research Center, NOVA Medical School, NOVA University of Lisbon, Rua Câmara Pestana 6, 1150-082 Lisbon, Portugal
- ² Unit of Imaging and Cytometry, Gulbenkian Institute of Science, Rua Quinta Grande 6, 2780-156 Lisbon, Portugal
- ³ Centre for Ecology, Evolution and Environmental Changes, Faculty of Sciences, University of Lisbon, Campo Grande, 1749-016 Lisbon, Portugal
- ⁴ Center for Proteomics and Metabolomics, Leiden University Medical Centre, Albinusdreef 2, 2333 ZA Leiden, The Netherlands

Introduction

The kidney is a vulnerable organ to xenobiotic toxicity due to its rich blood supply and its important role in drug metabolism and excretion. Proximal tubular cells are the primary sensor of either ischemic or oxidative renal injury as a consequence of their high metabolic rate and strong dependence on oxidative phosphorylation. Thus, it is consensual that mitochondrial damage plays a key pathogenic role in drug-induced renal injury (Basile et al. 2012; Chevalier 2016), which is partially explained by this dependence.

Animal experiments remain essential for understanding the mechanisms of drug toxicity and testing the safety of new compounds. However, rodent species, the most widely used animal model, predict only 41% of human toxicities (Olson et al. 2000) and are not useful for high throughput screenings. Thus, it is urgent to find better predictive

animal models that capture all the complexities of human physiology while enabling for testing large libraries of compounds. Zebrafish larvae up to 5 days of development have unique features that make them potentially excellent models in toxicology: transparency, rapid development, small size that allows them to fit in 96-well-plates, easy and fast drug administration in small amounts, no need for feeding, transgenic capabilities and high homology with mammals in terms of genetics, metabolism and physiology (McGrath and Li 2008; Peterson and MacRae 2012). Regarding the zebrafish kidney, the larval pronephros is fully mature at 4 days post-fertilization (dpf) and consists of two nephrons with the glomeruli fused at the embryo midline. Although simple in form, the glomerulus is composed of cell types that are typical of higher vertebrate kidneys, including fenestrated capillary endothelial cells and podocytes; the tubules are composed of polarized epithelial cells that exhibit primary cilia and possess a segmental organization where each segment is specialized for the secretion and reabsorption of particular molecules in a similar fashion as mammal nephron tubules (Kramer-Zucker et al. 2005; Wingert et al. 2007; Drummond and Davidson 2010). These features make zebrafish a potential model for nephrotoxicity assessment. Indeed, paracetamol and gentamicin, two drugs associated with renal tubular damage in man, (Mazer and Perrone 2008; Lopez-Novoa et al. 2011) have been proved to cause morphological and/or functional alterations in the zebrafish pronephros (Hentschel et al. 2005; Peng et al. 2010; Rider et al. 2012; Cianciolo Cosentino et al. 2013; Westhoff et al. 2013).

Herein, we aimed to evaluate the usefulness of zebrafish larvae as a model of tubular toxicity through a comprehensive analysis of the functional and morphological tubular alterations induced by three drugs known to cause tubulopathy in man: gentamicin, paracetamol and tenofovir in the form of tenofovir (TFV) and its prodrug tenofovir disoproxil fumarate (TDF) (Mazer and Perrone 2008; Smith et al. 2009; Lopez-Novoa et al. 2011).

Materials and methods

Zebrafish larvae

The transgenic and mutant zebrafish line Tg(wt1b:EGFP,cd h17:EGFP);mitfa^{-/-};roy^{-/+} or ^{+/+} was chosen for this study due to the expression of GFP at the renal tubules and transparency of the *nacre* mutant throughout the embryonic and larvae stages. Adult zebrafish were grown and mated at the Fish Facility of Gulbenkian Institute of Science, Lisbon, Portugal. Embryos were grown at 28 °C in embryo media of standard E3 solution (NaCl 5 mM, KCl 0.17 mM, CaCl₂ 0.33 mM, MgSO₄ 0.33 mM) plus HEPES buffer 10 mM till

4 dpf, time when zebrafish pronephros is completely mature (Kramer-Zucker et al. 2005).

Drug exposure

Gentamicin and paracetamol were purchased from Sigma-Aldrich. Tenofovir was administered in two forms: (a) the prodrug TDF, (b) TFV (Sequoia Research Products, UK). Stock solutions were prepared for all drugs at solubility concentrations: gentamicin 5000 µg/mL, paracetamol 12,000 µg/mL, TDF 6000 µg/mL and TFV 5000 µg/mL. All drugs except TFV were dissolved in sterile distilled water. TFV was prepared in embryo media. All stock solutions were aliquoted and stored at -20 °C till further use.

Zebrafish larvae of 4 dpf were transferred to 96-well-plates, 2 larvae per well. Embryo media was completely removed from each well and immediately after that, a specific volume of embryo media plus a specific volume of drug stock solution or drug vehicle (negative controls) were added into each well to achieve the desired drug concentration (total volume per well = 350 µL). Zebrafish larvae were incubated for 24 h at 28 °C.

Lethality curves

Lethality curves were defined with five or six different concentrations for each drug. Drug concentrations were empirically chosen to cover all lethality percentages: gentamicin 200, 600, 1000, 1400, 1800, 2200 µg/mL; paracetamol 2000, 2500, 3000, 3500, 4000, 4500 µg/mL; TDF 1000, 1500, 2000, 2500, 3000 µg/mL; TFV 2500, 3000, 3500, 4000, 4500, 5000 µg/mL. Ten larvae of four dpf were tested per each concentration in triplicate or quadruplicate. After drug exposure, all larvae were observed under a stereoscope (Nikon SMZ 745) to evaluate body curvature, tail-flip response, swimming pattern, heart oedema, heartbeat and necrosis. Lethality was defined as the absence of heartbeat and/or the presence of body necrosis. Percentages of lethality were calculated and plotted against the logarithm of drug concentration in micrometer. Lethal concentrations for 10% of the larvae (LC10) and curve slopes were manually obtained after probit transformation (Randhawa 2009). LC10 concentrations were used for the rest of the experiments.

Mass spectrometry for drug and metabolite identification

Pools of 50 zebrafish larvae of 4 dpf were exposed to the LC10 of paracetamol ($n = 10$), gentamicin ($n = 10$), TDF ($n = 10$), TFV ($n = 5$) or water ($n = 6$). After drug exposure, dead larvae were discarded and 40 larvae were transferred from each well to a clean Eppendorf. Larvae were immediately washed four times with cold water to remove

drugs and/or drug metabolites from the embryo media. After that, larvae were euthanized by rapid chilling to remove all remaining embryo media before snap freezing in liquid nitrogen to quench any enzymatic activity.

Metabolite extraction was performed with methanol:water 2:1 (Huang et al. 2013). The extracted supernatant was dried under vacuum and reconstituted in half volume of water for further injection into the RPLC-Q-TOF (UPLC Ultimate 3000 RS tandem LC system, Dionex, Amsterdam, The Netherlands; ESI-UHR-QqToF impact HD, Bruker Daltonics, Bremen, Germany). The details of the RPLC-Q-TOF method have already been reported (Nevodomskeya et al. 2011; Pacchiarotta et al. 2012).

Drugs and metabolites were identified by extracting the chromatograms of the expected m/z of the protonated drugs and/or metabolites of gentamicin (Clarot et al. 2004) paracetamol (Pacchiarotta et al. 2012) or TDF (Kurmi et al. 2016). To confirm those identifications, rational chemical formulas were generated based on the internally calibrated monoisotopic masses within 5 mDa mass error using the SmartFormula tool (version 4.2, build 395, Bruker Daltonics). Two parameters were registered for each ion-drug or metabolite assignment: mass error and mSigma. Only those m/z with an intensity >10,000 units in at least half of the samples were registered. MZmine version 2.3 was used to build the chromatograms for each drug and metabolite (Pluskal et al. 2010).

Assessment of renal function

Renal function was assessed with a modified clearance assay from Rider et al. (2012). The casper zebrafish line (*mitfa*^{-/-}; *roy*^{-/-}) was used for these experiments due to its transparency and absence of fluorescence. After LC10 exposure, live larvae were anesthetized with tricaine and injected with 1.4 nL of fluorescein isothiocyanate (FITC)-inulin 2.5% w/v in the duct of Cuvier. FITC intensity was imaged over the caudal region 10–15 min (baseline) and 2 h after injection (Zeiss Lumax V12). FITC intensity was quantified using the image-J software (Schindelin et al. 2015) selecting the area on the caudal artery between somites 16 and 18. Clearance of inulin was calculated as the percentage of decrease of FITC intensity on the caudal artery using the formula (FITC intensity at baseline – FITC intensity at 2 h) * 100/ FITC intensity at baseline. A minimum of 15 larvae were injected per group.

Two-photon microscopy for evaluation of tubular morphology

After LC10 exposure, Tg(*wt1b:EGFP,cdh17:EGFP*); *mitfa*^{-/-}; *roy*^{-/+ or +/+} zebrafish larvae were fixed overnight with PFA 4% and washed with PBS 1X. Due to the central localization

of the pronephros, zebrafish larvae were further processed for imaging by removing the head, yolk and gut with a sharp needle and bistoury. This procedure was easily performed under a fluorescent stereoscope because our transgenic zebrafish expressed GFP in the pronephros and the gut. In a Petri dish with a base of 2% agarose, the remaining tissue was mounted in a drop of low melting agarose 1% and oriented with the ventral side up. The Petri dish was filled with PBS 1X. Embryos were then imaged on a Prairie Multi-Photon microscope equipped with an Olympus 20× XLUMP-LAN FL N (NA 1) water immersion lens and laser tuned to 890 nm. Stacks were obtained with 0.7 μm sectioning and further pre-processed with the FIJI software (Schindelin et al. 2012). Four or five larvae were imaged for each condition. 3D reconstructions of the proximal convoluted tubule were performed using the Amira software (version 5.3.3). For the lumen caliber measurement, two orthogonal diameters were measured in transverse planes of the lumen at regular intervals along all the reconstructed proximal convoluted tubule (PCT). Both diameters were divided by two to obtain the radius and the formula $\pi \times \text{radius}^2$ was applied to calculate the transverse section area of the lumen. An average of 15 measurements was done per larvae across one PCT.

Transmission electron microscopy for evaluation of tubular mitochondria

After LC10 exposure, Tg(*wt1b:EGFP,cdh17:EGFP*); *mitfa*^{-/-}; *roy*^{-/+ or +/+} zebrafish larvae were euthanized by rapid chilling. Larvae were fixed following a modified protocol from Schieber et al. (2010). In brief, larvae were fixed overnight with 2.5% glutaraldehyde and 2% PFA in 0.1 M of PHEM buffer. In a Pelco BioWave Microwave Processor (Ted Pella, Redding USA), larvae were post-fixed in 1% osmium tetroxide (EMS, Hatfield, PA, USA) in 0.1 M of PHEM Buffer on ice, and en-block stained with 1% of aqueous uranyl acetate (EMS, Hatfield, PA, USA) before being dehydrated in a graduated ethanol series and embedded in EPON resin (EMS, Hatfield, PA, USA). Larvae were left in 100% EPON resin overnight before orientation, embedding and resin polymerization in a 60 °C oven. All larvae were processed simultaneously except gentamicin-treated larvae.

Transverse portions of the proximal convoluted tubule were serial sectioned at 70 nm (for micrographs), 100 nm (for serial section TEM (ssTEM)) or 120 nm (for tomography) with a diamond knife (Diatome, Biel Switzerland) on a Reichert Ultracut S (Leica, Vienna, Austria). 10 nm of Protein A Gold was added (UMC, Utrecht, The Netherlands) to the grids for tomography analysis. All grids were post-stained with uranyl acetate and lead citrate.

Data was collected on a Hitachi H-7650 Transmission Electron Microscope (Tokyo, Japan) at 100 kV using three

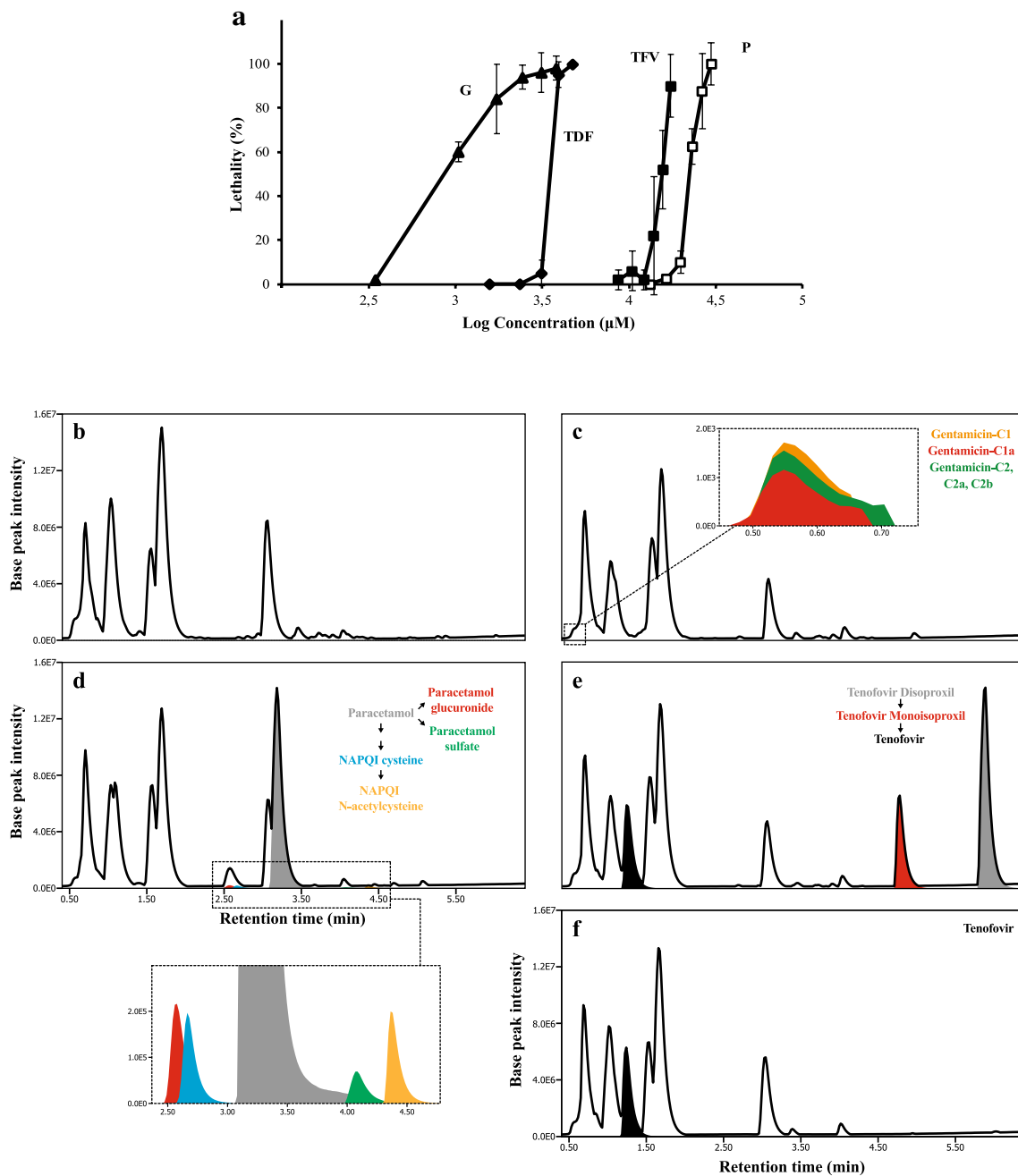


Fig. 1 Zebrafish exposure to LC10. **a** Lethality curves that were obtained to calculate the LC10 of gentamicin (G), tenofovir disoproxil fumarate (TDF), tenofovir (TFV) and paracetamol (P). **b** Chromatogram of untreated zebrafish larvae. **c** Chromatogram of zebrafish exposed to gentamicin; a zoom of the chromatogram shows the extracted ion chromatograms (EICs) for [gentamicin C1+H]⁺ (*m/z* 478.3231), [gentamicin C2 C2a and C2b+H]⁺ (*m/z* 464.3076) and [gentamicin C1a+H]⁺ (*m/z* 450.2920). **d** Chromatogram of zebrafish exposed to paracetamol showing the EIC of [paracetamol+H]⁺ (*m/z*

152.0706), [paracetamol glucuronide+H]⁺ (*m/z* 328.1029), [paracetamol sulfate+H]⁺ (*m/z* 232.0275), [paracetamol cysteine+H]⁺ (*m/z* 271.0748) and [paracetamol *N*-acetylcysteine+H]⁺ (*m/z* 313.0858); a zoom of the chromatogram shows in more detail the four paracetamol metabolites. **e** Chromatogram of zebrafish exposed to TDF showing the EIC of [tenofovir disoproxil+H]⁺ (*m/z* 520.1808), [tenofovir monoisoproxil+H]⁺ (*m/z* 404.1336) and [tenofovir+H]⁺ (*m/z* 288.0857). **f** Chromatogram of zebrafish exposed to TFV showing the EIC of [tenofovir+H]⁺ (*m/z* 288.0859)

approaches: (1) micrographs at a magnification of 1K, 3K, and 10K (a minimum of 50 tubular cells were screened from 10 to 20 micrographs per condition); (2) ssTEM to build

coarse cellular 3D models with 24 or 36 micrographs covering an area of $\sim 10 \times 11 \times 2.4 \mu\text{m}$ or $3.6 \mu\text{m}$; (3) tomograms to build 3D mitochondrial models for an area of

$3.8 \times 4.4 \times 0.36 \mu\text{m}$ and with an angle range from -55° to 55° , with a 1° tilt increment. Data were aligned and modeled with the IMOD software (Kremer et al. 1996; Mastronarde 1997). Due to the complexity of the 3D modeling, only one cellular model and one mitochondrial model were built for each condition. However, those models were carefully chosen to be the best in describing the changes observed from each condition (supplementary videos).

Mitochondrial swelling was assessed by measuring mitochondria grey intensities from 14 to 24 mitochondria from a total of three micrographs using the FIJI software. Mitochondrial granules were counted from 11 to 18 mitochondria from a total of three micrographs using the FIJI software. The volumes of the mitochondria, cristae and granules were measured with the IMOD software and expressed as percentage of the cellular or mitochondrial volume captured by the 3D model. All analyses were performed at the same time for the five different conditions of the study.

Statistical analysis

Statistical analyses were performed with SPSS (IBM SPSS Statistics for Windows, version 22.0. Armonk, NY: IBM Corp). Differences in quantitative variables among treatment groups were analyzed with one-way ANOVA test followed by Games-Howell post hoc test. All parameters were expressed as means and standard deviation. P values <0.05 were considered statistically significant.

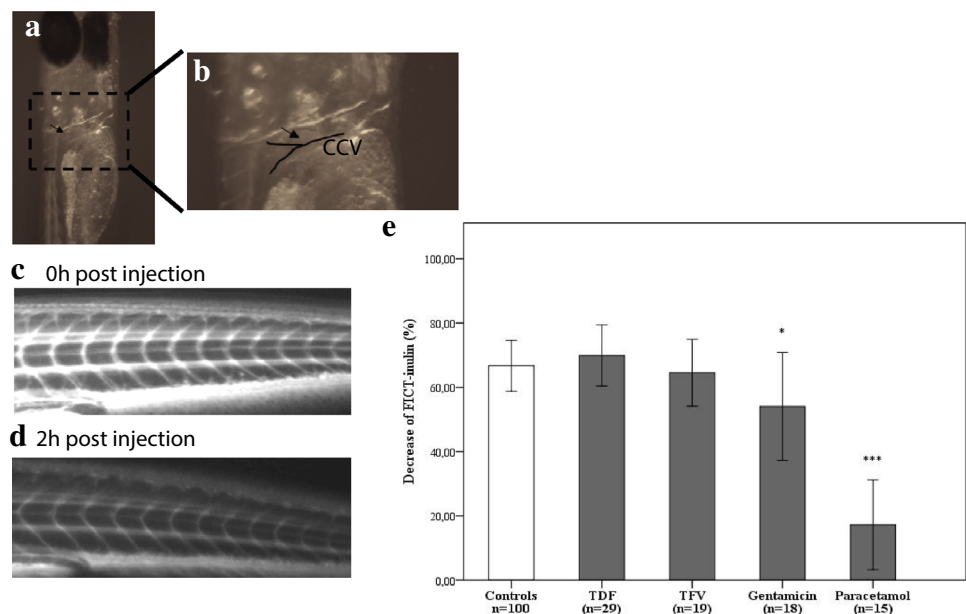
Results

Lethality curves

After 24 h of exposure to each drug concentration, zebrafish larvae were observed under a stereoscope for macroscopic alterations. Swimming behavior was reduced and the escape response to tail stimuli was retarded or absent in living larvae exposed to any drug concentration when compared with control larvae. Albeit rarely, some larvae exposed to the second-fourth drug concentrations (in ascendant order) experienced upwards body curvature and/or heart oedema with visible heart hemorrhage. Dead larvae presented (i) no heartbeat with no necrosis at the lowest lethal concentrations or (ii) necrosis and body decomposition at the highest lethal concentrations (data not shown).

The percentages of lethality were calculated for each drug concentration and plotted against the logarithm of the drug concentration (Fig. 1a). Regarding the left–right position of the curves, the order of the drugs was gentamicin, TDF, TFV and paracetamol. LC10 (μM) calculated from the lethality curves after probit transformation were: 491 for gentamicin, 2338 for TDF, 11,542 for TFV, and 17,179 for paracetamol. All drugs exhibited sigmoidal lethality curves but with different slopes. Paracetamol, TDF and TFV curves were steeper than gentamicin curve as reflected by the values of the slopes (% of lethality/ μM): 12 for paracetamol, 10 for TDF, 9 for TFV and 4 for gentamicin.

Fig. 2 Renal clearance is decreased in zebrafish larvae exposed to the LC10 of gentamicin and paracetamol. **a, b** Detail of the common cardinal vein (CCV) where inulin-FITC was injected to evaluate the renal clearance. **c, d** Lateral posterior view of the FITC intensity in blood 10–15 min (**c**) and 2 h (**d**) after FICT-inulin injection. **e** Clearance of inulin, expressed as the percentage of decrease of FITC intensity in blood 2 h after FICT-inulin injection, is decreased with gentamicin and paracetamol



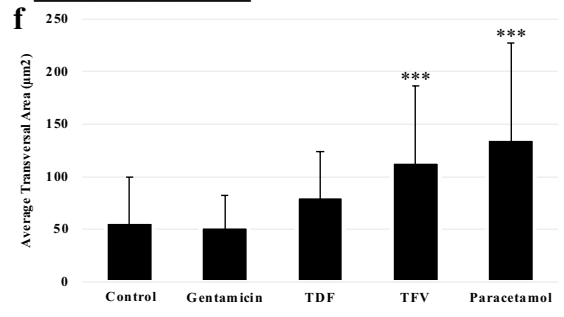
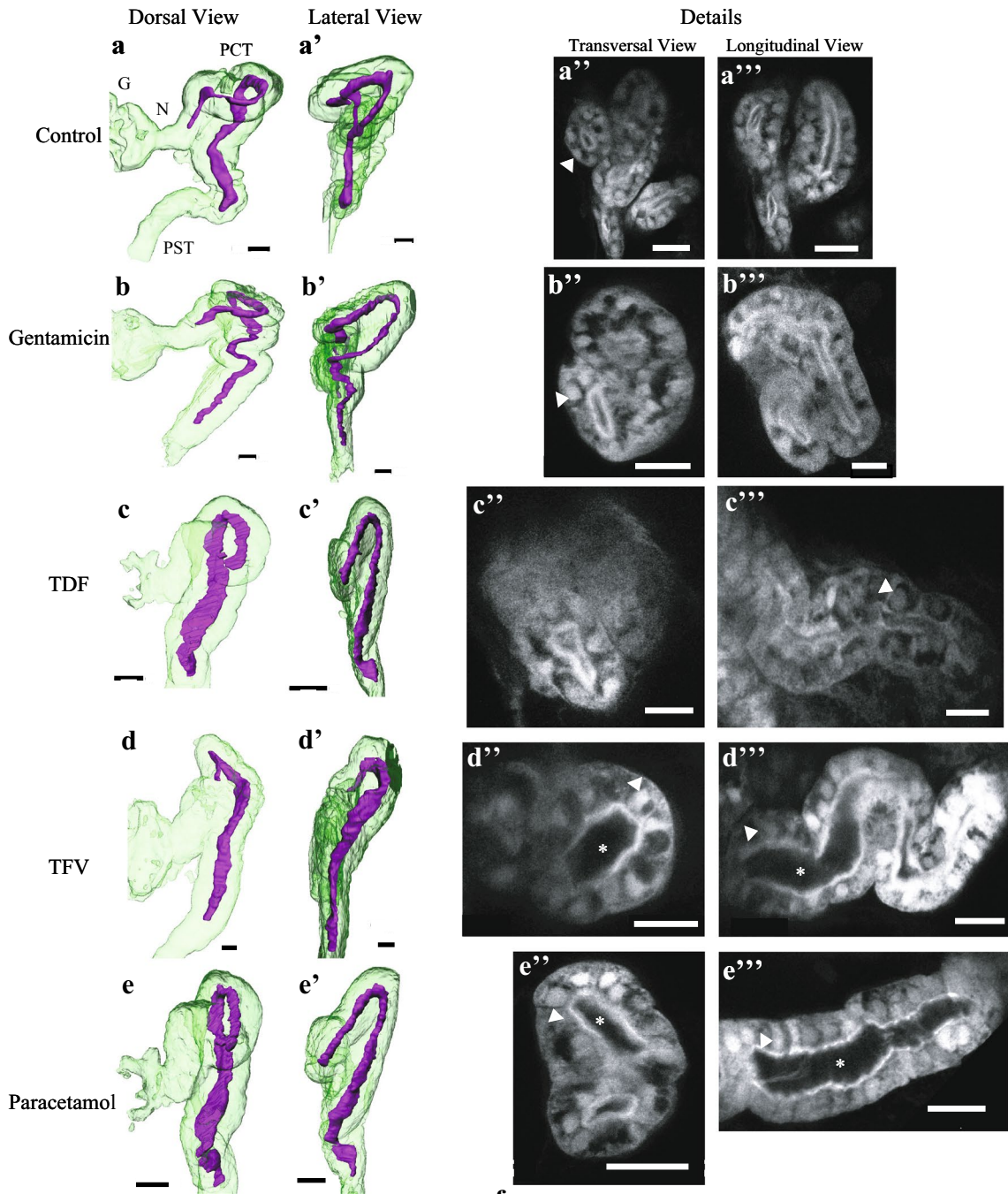


Fig. 3 The lumen of the proximal convoluted tubules is enlarged in zebrafish larvae exposed to the LC10 of TFV and paracetamol. **a, a', b, b', c, c', d, d', e, e'** Dorsal and lateral views of the proximal convoluted tubule of untreated larvae and larvae exposed to the LC10 of gentamicin, TDF, TFV or paracetamol. Compared to controls, the complexity of the coiled structure of the proximal convoluted tubules is reduced in the treated zebrafish larvae. **a'', a''', b'', b''', c'', c''', d'', d''', e'', e'''** Transversal and longitudinal amplifications of the proximal convoluted tubule of untreated larvae and treated larvae exposed to LC10 of gentamicin, TDF, TFV or paracetamol. GFP labels the nuclei and the membrane of the tubular cells. **d'', d''', e'', e'''** The lumen of the tubule is enlarged in zebrafish exposed to TFV and paracetamol. **f** Transversal area of the proximal convoluted tubules. Scale: 20 μm . G: glomeruli; N: nuclei; PCT: proximal convoluted tubule; PST: proximal straight tubule. White asterisks mark tubule enlargements; white arrowheads show misplaced nuclei. ***For p value <0.001

Identification of drugs and metabolites in zebrafish larvae

To test if drugs were absorbed and followed similar biotransformation patterns as in man, extracts of whole zebrafish larvae exposed to the LC10 of each drug were analyzed by mass spectrometry.

Chromatograms of zebrafish exposed to paracetamol showed all known paracetamol metabolites found in man. We detected phase II metabolites derived from conjugation with glucuronic acid and sulfonic acid and paracetamol metabolites derived from the unstable and toxic phase I metabolite *N*-acetyl-*p*-benzoquinone imine (NAPQI) after conjugation with glutathione (Fig. 1d).

Chromatograms of zebrafish exposed to TFV showed only the peak corresponding to TFV (Fig. 1f). No traces were found for the intracellular phosphorylated metabolites of tenofovir. Regarding the prodrug of TFV, the chromatograms of zebrafish larvae exposed to TDF included the diester tenofovir disoproxil, the monoester tenofovir monoisoproxil and its non-esterified metabolite TFV (Fig. 1e). The retention time and mass spectrum of TFV were similar to the ones described for zebrafish exposed to TFV (Fig. 1f; Supplementary Tables 2 and 3). In-source fragmentation occurred for paracetamol, TFV, TDF and their respective metabolites, which confirmed their identifications (Supplementary Tables 1–3).

Finally, zebrafish larvae exposed to gentamicin sulfate produced chromatograms that were unexpectedly identical to the chromatograms of untreated larvae (Fig. 1b, c). The *m/z* of the five major components of gentamicin (C1, C1a, C2, C2a and C2b gentamicin) were found in the spectra from zebrafish larvae exposed to gentamicin but the intensities were <2000 units in all samples (Fig. 1c). In-source fragmentation (to *m/z* 322.1963 and 160.0966) was detected but with intensities between 2000 and 10,000 units.

Renal function

Renal function was evaluated with the inulin clearance assay after exposure to the LC10 of each drug.

Two hours after FITC-inulin injection, FITC intensity decreased by $67 \pm 8\%$ in untreated larvae ($n = 100$) due to glomerular filtration of most of the FITC-inulin present in the blood (Fig. 2e). Larvae exposed to gentamicin ($n = 18$) or paracetamol ($n = 15$) had significantly lower clearances with 54 ± 17 and $17 \pm 14\%$ of decrease of FITC intensity, respectively. TDF ($n = 29$) or TFV ($n = 19$) treatments did not affect inulin clearance (69 ± 9 and $64 \pm 10\%$, respectively).

Microscopic alterations

General tubular morphology, epithelium organization and luminal area of the proximal convoluted tubule (PCT) were carefully compared between controls and treated larvae using 3D reconstructions.

Untreated zebrafish larvae showed PCT as coiled and intricate structures with a typical curvature. At the exit of the glomeruli, each of the PCT came dorsally and distally before curving ventrally and to the middle. Then, it continued posteriorly with several undulations or convolutions until the proximal straight tubule (PST) (Fig. 3). The two tubules were symmetric and diverged from each other at the exit of the glomerulus and then were brought closer from the beginning of the PST (Fig. 3). The fluorescent transgenic line *cdh17:EGFP* and *wt1b:EGFP* revealed a single layer of tightly packed epithelial cells surrounding the lumen of each tubule. Apical membranes were enriched with cadherin 17 (here seen by fusion with EGFP) and showed cells with a regular shape. The fluorescence from *wt1b:EGFP* reporter showed big nuclei, usually in the basal portion of the cell (Fig. 3a'', a'''). The lumen caliber of the PCT had a mean area of $57 \pm 43 \mu\text{m}^2$, with some variations throughout the length of the PCT (Fig. 3f).

In general, there were no apparent differences regarding the curvature of the tubules between treated and untreated larvae, except for the terminal section of the PCT, which presented a simplified structure with less curves upon drug exposure (Fig. 3a'–e'). Tubular enlargements were observed with all drugs except gentamicin ($53 \pm 29 \mu\text{m}^2$, Fig. 3f). Paracetamol showed irregular lumens and the most severe dilations with an average area of $136 \pm 92 \mu\text{m}^2$ (white asterisks in Fig. 3f, e'', e''') followed by TFV with $114 \pm 73 \mu\text{m}^2$ (Fig. 3d'', d'''). TDF-treated larvae showed milder defects with more regular lumens. The lumen was also dilated compared to controls but the increase was not statistically significant ($81 \pm 71 \mu\text{m}^2$, Fig. 3f).

Paracetamol, TDF and TFV lead to epithelium disorganization with displaced nuclei towards the middle portion of the cell (Fig. 3e'', e''', d'', d''', c'', c''').

Tubular mitochondrial alterations

Mitochondria morphology was evaluated using three different approaches: micrographs, serial section transmission electron microscopy 3D reconstructions of proximal tubular cells, and tomographic 3D reconstructions of mitochondria.

Micrographs from control larvae showed mitochondria as tubular organelles with smooth contours and regular shapes differing in size (Fig. 4b–b’). 3D cellular models enabled us to notice that they were interconnected, forming a vast mitochondria network (Fig. 5b’). Cristae were thin and long cylindrical structures distributed throughout the mitochondrion in different orientations. They branched from several places creating bridges that interconnected with each other (Fig. 5m’). Matrix granules occurred outside the cristae as tiny electron dense puncta.

3D cellular models revealed changes in mitochondria shape and size from drug-exposed larvae. Gentamicin and TFV caused “donut”-like shapes (Fig. 5g). Paracetamol caused “pancake”- (Figs. 4d”, 5h) and “rod”-like shapes (Fig. 5i). TDF and TFV-produced mitochondria with irregular contours (Fig. 5j) and huge mitochondria (Fig. 5k). There were no differences in the volume occupied by mitochondria (Supplementary Table 4). However, mitochondrial electron densities were significantly lower in gentamicin, TDF and TFV than in controls (141 ± 6 in controls, gentamicin 172 ± 5 , TDF 161 ± 6 , TFV 163 ± 6) (Fig. 4g). These results are in agreement with the enlarged mitochondria that were seen in the micrographs and 3D cellular models of gentamicin, TDF and TFV (Figs. 4c”, e”, f”, 5k).

3D mitochondrial models showed no differences in the volume occupied by cristae (Supplementary Table 4). However, cristae from treated larvae, were clearly fragmented and/or degraded when compared with control larvae (Figs. 4c”, e”, f”, 5n’, o’, p’ q’).

The number of mitochondrial granules was reduced in all treated larvae, although it was only statistically significant for gentamicin, TDF and TFV (5 ± 2 granules/mitochondrion in controls, 0.7 ± 0.4 in gentamicin, 3 ± 1 in paracetamol, 2 ± 0.9 in TDF $p = 0.031$, 2 ± 1 in TFV) (Fig. 4h). The volume occupied by granules from each representative mitochondrion 3D model was also reduced in all treated larvae (Supplementary Table 4).

Discussion

In the present study, acute toxicity was induced in zebrafish by three drugs associated with tubular damage in man. For all tested drugs, morphological and/or functional tubular alterations were found, which supports the usefulness of the zebrafish model to evaluate tubular toxicity.

Physiological and biochemical characterization of zebrafish is of utmost importance to support its use in toxicology studies. Vertebrate kidneys play essential roles in the excretion of metabolic waste products and in the maintenance of the internal electrolyte and acid–base balances. Similarly to man, the nephron of zebrafish larvae consists of a glomerulus, responsible for blood filtration, followed by a renal tubule and duct, which are responsible for solute reabsorption and secretion (Drummond and Davidson 2010). Likewise, the zebrafish tubular epithelium expresses ion channels, transporters and claudins in a segment-specific manner that confer unique absorptive and secretory properties to each nephron segment. Among other examples, the PCT expresses the Na^+ /bicarbonate cotransporter *Slc4a4a* and the endocytic receptors *megalyn* and *cubilin*; the distal early tubule (equivalent to the human thick ascending limb) expresses the Na^+ / Cl^- / K^+ cotransporter *Nkcc2*; the distal late tubule (equivalent to the human distal convoluted tubule) expresses the Na^+ / Cl^- cotransporter *Ncc* (Kersten and Arjona 2017). Information about regulation of renal ion transport in zebrafish is limited, but the renin–angiotensin system plays a very important role in the control of Na^+ reabsorption (Kumai et al. 2014; Rider et al. 2015). Despite these similarities, functional differences exist between zebrafish and human nephrons: (i) absence of water-absorptive segments such as the human thin descending limb because freshwater fish do not need to concentrate urine; (ii) absence of aldosterone (although zebrafish have mineralocorticoid receptors); (iii) presence of unique structures with no clear human counterpart such as the Corpuscle of Stannius, a renal gland involved in the regulation of calcium and phosphate levels potentially linked with the human macula densa (Wingert and Davidson 2008; Kersten and Arjona 2017).

ADME processes have been insufficiently characterized in zebrafish and are restricted to some metabolizing enzymes and membrane transport proteins. Phase I (CYPs) and phase II (UGT1A1, SULTs) enzymes have been identified (Hill et al. 2012), but most of functional information is only known for CYPs. The genetic homology of the most relevant CYPs between zebrafish and man is diverse. While there are orthologous relationships for most of CYP1s and CYP3s, only 26 from the 46 zebrafish CYP2s genes have human CYP orthologs (Goldstone et al. 2010). In line to what is well known in man, the expression of most of CYPs throughout zebrafish development is variable. With regards to CYP activity, zebrafish and human CYPs share some substrates, inhibitors and inducers. Moreover, some of those inducers proved to be agonists of the zebrafish pregnane X receptor (PXR) or aryl hydrocarbon receptor, which suggest common regulatory pathways of CYPs expression. However, there are important differences in the response to many substrates, inducers and inhibitors as reviewed by

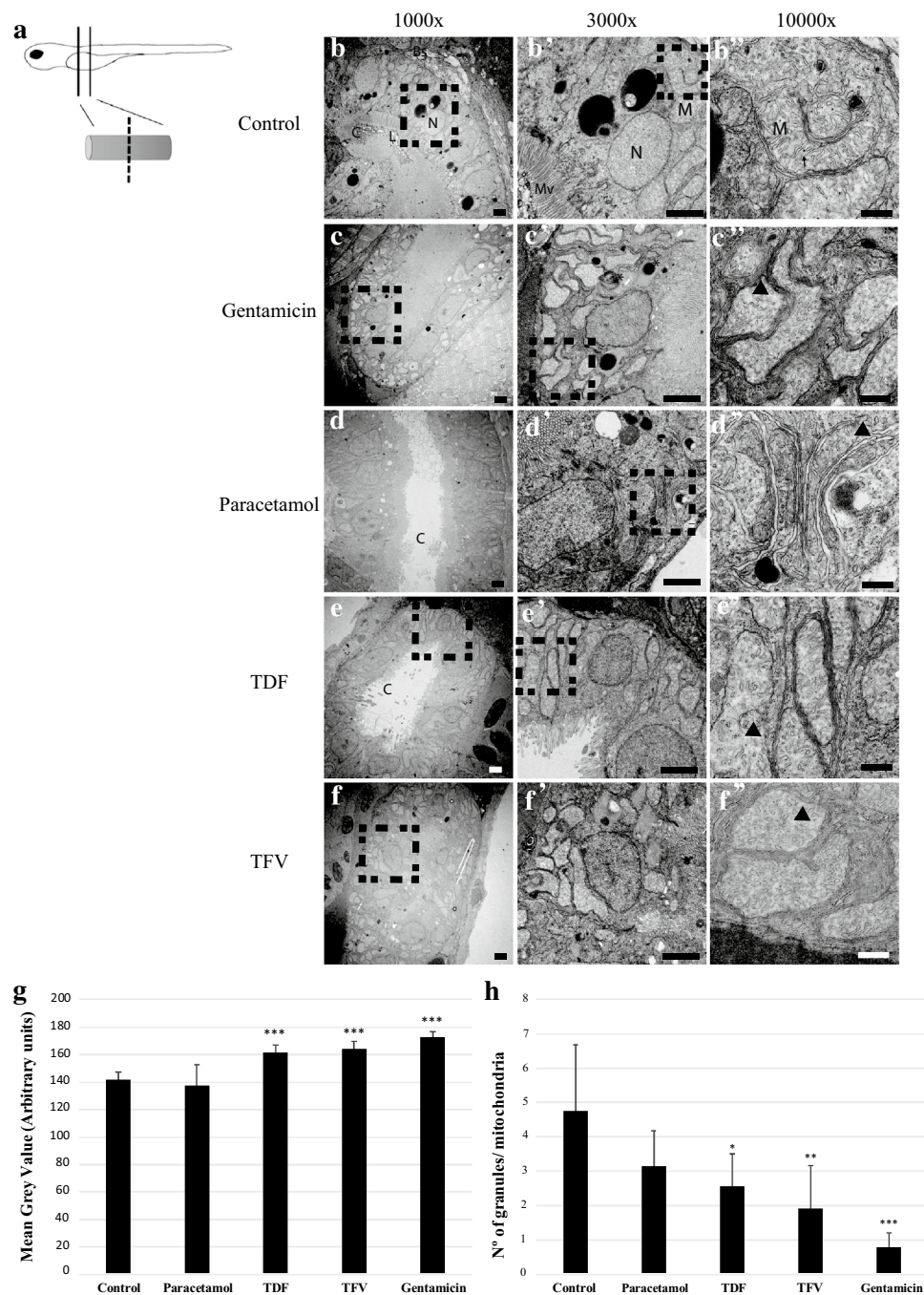
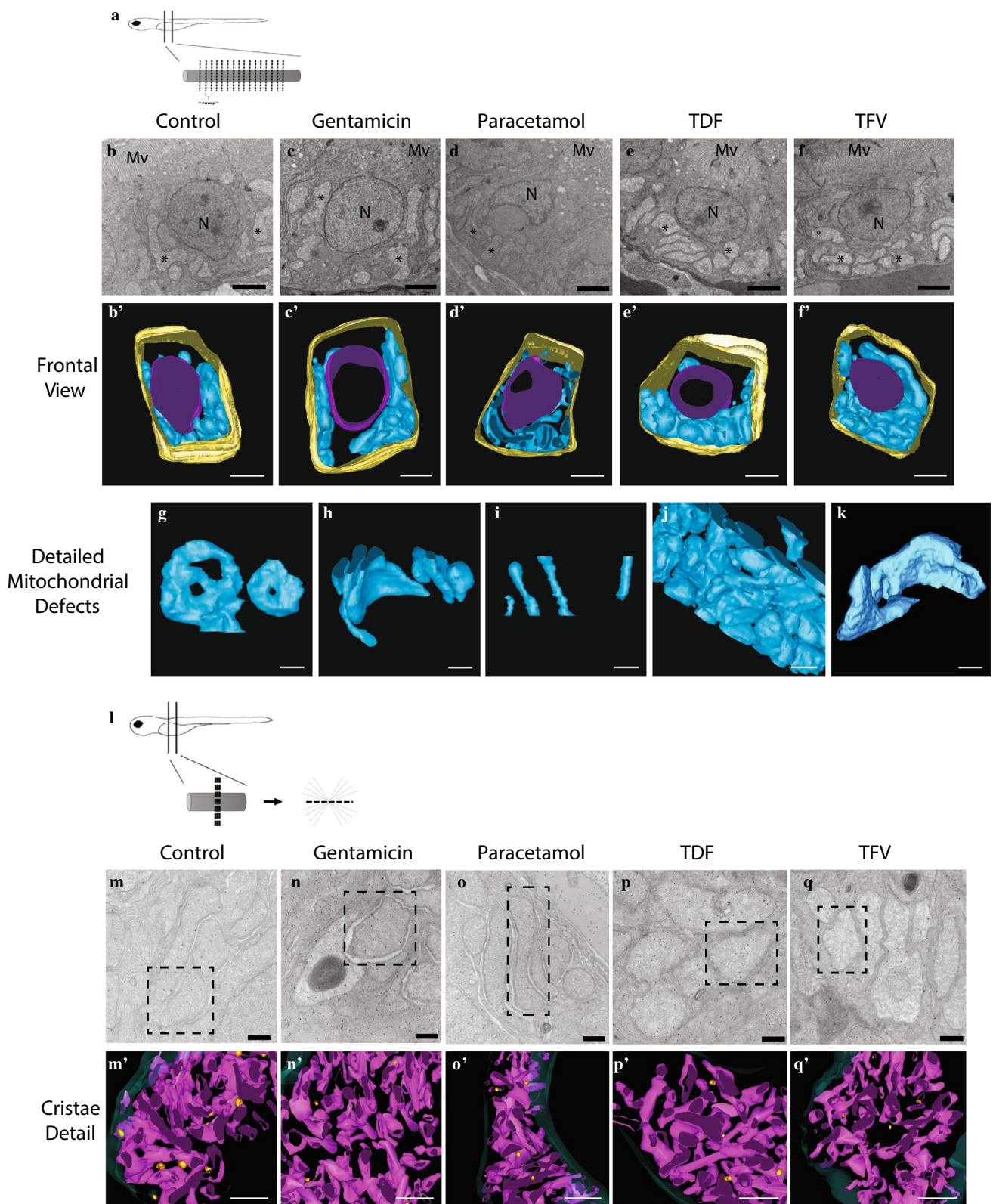


Fig. 4 Mitochondrial morphological alterations in electron micrographs after exposure to the LC10 of gentamicin, paracetamol, TDF and TFV. **a** Scheme of the sectioning of the proximal convoluted tubule for single micrographs; each section had a z of 70 nm. **b–f** Micrographs at 1000 \times showing the proximal tubular epithelium as one cell layer with the basal membrane leading to blood and the apical membrane ending in microvilli that gave into the lumen of the tubule. **b'–f'** Micrographs at 3000 \times showing one proximal tubular cell with the nucleus in the center and the mitochondria in the basal and lateral sides for all condition. **b''–f''** Micrographs at 10,000 \times showing some mitochondria. Thin and long mitochondria such as “pancakes” are seen in larvae exposed to paracetamol. Swollen mito-

chondria are observed in larvae exposed to gentamicin, TDF and TFV. Mitochondria cristae are fragmented and mitochondria granules are missing in all treated larvae. **g** The mean gray intensity reveals mitochondrial swelling in larvae exposed to gentamicin, TDF and TFV. **h** Mitochondrial granules are decreased by all drugs and significantly for gentamicin, TDF and TFV. Scale: 1000 \times –2 μ m; 3000 \times –2 μ m; 10000 \times –500 nm. Bs: basolateral membrane; C: cilia; L: lumen; Mv: microvilli; M: mitochondria; N: nucleus. Arrows mark granules; arrow heads mark fragmented cristae; asterisks mark phospholipidosis; square boxes, when present, indicate the area that was zoomed in and presented in the next image. *For p value <0.05, **for p value <0.01, ***for p value <0.001



Saad et al. (2016). Membrane transport proteins involved in the uptake and excretion of drugs and/or metabolites (i.e. SLC, ABC proteins) are also present in zebrafish. The most

relevant ABC drug efflux pumps in man, namely ABCB1, ABCC1-5 and ABCG2, are expressed in zebrafish tissues that are involved in absorption, excretion or serving as a

Fig. 5 Mitochondrial morphological alterations in ssTEM and tomograms after exposure to the LC10 of gentamicin, paracetamol, TDF and TFV. **a** Scheme of the serial sectioning of the proximal tubule for ssTEM to build 3D cellular models; 24–36 sections were cut for each ssTEM with a z of 100 nm per section. **b–f** Micrographs at 3000 \times showing the cell that was chosen to build the cellular 3D representative model for each condition. **b'–f'** Frontal section of the cellular 3D model for each condition. **g–k** Weird mitochondrial shapes caused by the drugs: **(g)** “donuts” with gentamicin, **(h)** “pancakes” with paracetamol, **(i)** “rods” with paracetamol, **(j)** fragmented mitochondria with irregular shapes with TDF and TFV, **(k)** huge mitochondria occupying a big part of the cytosol with TDF and TFV. **l** Scheme of the serial sectioning of the proximal tubule for tomograms to build 3D mitochondrial models; three sections were cut for each tomogram with a z of 120 nm per section. **m–q** Micrographs at 8000 \times with Protein A Gold showing the mitochondrion that was chosen to build the representative mitochondrial 3D model for each condition. **m'–q'** Frontal section of the mitochondrial 3D model for each condition; cristae are fragmented in drug treated larvae. Scale: **b–f**—2 μ m; **b'–f'**—2.5 μ m; **g–k**—1 μ m; **m–q**—500 nm; **m'–q'**—95 nm

barrier function (intestine, liver, kidney, gills, brain blood barrier). Interestingly, despite the lack of data about transcriptional regulation of ABC transporters, an association was found between PXR, CYP3A and ABCB1 in zebrafish (Luckenbach et al. 2014). This example supports a similar regulation of detoxification enzymes and transporters between zebrafish and man.

Due to the limited information about pharmacokinetics in zebrafish, we assessed the drug metabolic profile of 5-day zebrafish larvae. In the case of paracetamol, all metabolites were detected except NAPQI and paracetamol glutathione probably due to their high instability (Cook et al. 2015). Upon these results, we can conclude that zebrafish and man share the same pathways for paracetamol metabolism: glucuronidation, sulfonation and oxidation with posterior detoxification to paracetamol *N*-acetylcysteine. In the case of TDF, MS experiments identified tenofovir monoisoproxil and TFV in zebrafish extracts. TDF follows enzymatic hydrolysis through not only intestinal and blood esterases but also non-enzymatic hydrolysis in water (Kurmi et al. 2016). Although we cannot exclude the possibility of some TDF hydrolysis in the embryo media, zebrafish expresses esterases (Levi et al. 2012), which supports TDF metabolism in zebrafish. TFV phosphorylated metabolites were not detected in zebrafish exposed to either TFV or TDF. Zebrafish expresses both organic anion transporters, necessary for intracellular TFV uptake, and nucleotide kinases, necessary TFV phosphorylation (Pannicke et al. 2009; Mihaljevic et al. 2016). Thus, a plausible explanation for the absence of TFV metabolites might be related with technical limitations of our extraction or LC–MS methods. Finally, gentamicin, which is not metabolized, was present in the zebrafish extracts but at very low concentrations probably due to its low bioavailability (Gemer et al. 1983).

Renal clearance was decreased by 19 and 74% by gentamicin and paracetamol, respectively. Drugs can decrease renal clearance by different mechanisms that do not necessarily involve damage to the renal parenchyma. For instance, drugs that inhibit renal prostaglandin-mediated vasodilation such as paracetamol (Graham and Scott 2005) and gentamicin (Lopez-Novoa et al. 2011) and hepatotoxic drugs such as paracetamol (Mazer and Perrone 2008) can decrease renal clearance. Neither the liver nor the renal blood flow were evaluated in this work but previous studies found that gentamicin decreases the venous erythrocyte velocity and the heart rate in zebrafish larvae (Hentschel et al. 2005; Rider et al. 2012). Besides these indirect mechanisms, drugs that directly damage the glomeruli and/or the renal tubule can also decrease the renal clearance via several mechanisms (Basile et al. 2012). In this study, all tested drugs caused morphological tubular alterations but only gentamicin and paracetamol reduced inulin clearance. Interestingly, similar results are seen in men: HIV patients on TDF can develop proteinuria, a specific marker of tubular injury, with normal values of glomerular filtration rate (Tourret et al. 2013). Thus, tubular morphological alterations associated with TFV seem to precede the decline in the renal clearance. In the case of gentamicin and paracetamol, a combination of their intrinsic tubular effects and their potential pre-renal effects could explain the observed decrease in renal clearance. Besides, gentamicin can cause intraglomerular mesangial cell contraction (Lopez-Novoa et al. 2011), which can also decrease the renal clearance.

The intrinsic complexity of the PCT represented a big challenge for imaging. Previous works applied confocal or conventional optical microscopy to image the pronephros but with poor quality results (Peng et al. 2010; Westhoff et al. 2013). We provide for the first time exhaustive imaging of the PCT that allowed building 3D images to objectively measure the caliber of the tubular lumen. Paracetamol, TDF and TFV induced tubular dilatations and epithelium disorganization with nuclei delocalization. Tubular dilatations are one of the earliest morphological alterations of acute tubular injury followed by loss of cytoskeletal integrity and cell polarity (Bonventre and Yang 2011; Basile et al. 2012). We did not perform any immunostaining for apical or basal markers but epithelium and nuclei disorganization found in our study could be associated with the loss of cell polarity.

The loss of the structure of the tubular epithelium is associated with ATP depletion and thus mitochondrial damage (Price 2002; Basile et al. 2012). Mitochondrial morphology is highly variable and dynamic due to the ability of mitochondria to undergo the highly coordinated processes of fusion and fission. Mitochondrial fusion allows the exchange and complementation of partially damaged mitochondria contents when the stress is

below a critical threshold, while mitochondrial fission is required to remove damaged mitochondria during high levels of stress (Youle and van der Bliek 2012; Rafelski 2013). Thus, quantification of mitochondria volume and number can be regarded as a measure of the insult intensity. We provide for the first time 3D models of PCT cells and mitochondria. These models were very useful to understand the complexity of mitochondria networks, to get accurate measurements of mitochondria volume and number and to identify alterations in mitochondria shape and cristae fragmentation. However, because 3D modeling at the ultrastructural level is a laborious task, only one model was made for each condition. Although each model was carefully chosen to represent each condition, there were a substantial number of mitochondria that were not fully captured by the models. Thus, we cannot conclude about drug-induced changes in the volume or number of mitochondria.

Drug-induced mitochondrial defects were manifested as: mitochondrial shape alterations including “donuts” with gentamicin and TFV in comparison to “pancakes” and “rods” with paracetamol; mitochondrial size alterations in the form of mitochondrial swelling with gentamicin, TDF and TFV; mitochondrial cristae fragmentation and reduction in the number of mitochondrial granules with all drugs. Mitochondrial morphological alterations have a direct impact on mitochondrial functions, which are vital for cellular functioning, from ATP generation to regulation of apoptosis (Galloway and Yoon 2012). For example, mitochondrial swelling, considered to be an early sign of functional deterioration of the organelle, is an indicator of the opening of the mitochondrial permeability transition pore (Arpagaus et al. 2002; Herlitz et al. 2010). Thus, mitochondrial swelling together with cristae damage can result in a disruption of the electron transport chain, leading to a decrease in the ATP production.

In conclusion, this work demonstrates the high homology between zebrafish and mammals for drug metabolism and drug-induced morphological and functional tubular alterations. Together, these results support the use of zebrafish in toxicological studies.

Acknowledgments We would like to thank Maysa Franco and Ana Cristina Borges from the Fish Facility of the Gulbenkian Institute of Science.

Compliance with ethical standards

Funding This work was supported by the Calouste Gulbenkian Foundation, Gulbenkian Professorship 121986/2012; the Foundation for Science and Technology through the grant ANR/BEX-BID/0153/2012, contract IF/00951/2012 (to SSL), fellowship PD/BD/52420/2013 (to RJ) and travel ship SFRH/BSAB/114291/2016 (to JM); iNOVA4Health Research Unit, LISBOA-01-0145-FEDER-007344.

Ethical statement All procedures performed in studies involving animals were in accordance with the ethical standards of the institution or practice at which the studies were conducted.

Conflict of interest The authors declare that they have no conflicts of interest.

References

- Arpagaus S, Rawlyer A, Braendle R (2002) Occurrence and characteristics of the mitochondrial permeability transition in plants. *J Biol Chem* 277:1780–1787
- Basile D, Anderson M, Sutton T (2012) Pathophysiology of acute kidney injury. *Compr Physiol* 2:1303–1353
- Bonventre J, Yang L (2011) Cellular pathophysiology of ischemic acute kidney injury. *J Clin Invest* 121:4210–4221
- Chevalier RL (2016) The proximal tubule is the primary target of injury and progression of kidney disease: role of the glomerulotubular junction. *Am J Physiol Renal Physiol* 311:F145–F161
- Cianciolo Cosentino C, Skrypnik NI, Brilli LL et al (2013) Histone deacetylase inhibitor enhances recovery after AKI. *J Am Soc Nephrol* 24:943–953
- Clarot I, Chaimbault P, Hasdenteufel F et al (2004) Determination of gentamicin sulfate and related compounds by high-performance liquid chromatography with evaporative light scattering detection. *J Chromatogr A* 1031:281–287
- Cook SF, King AD, van den Anker JN, Wilkins DG (2015) Simultaneous quantification of acetaminophen and five acetaminophen metabolites in human plasma and urine by high-performance liquid chromatography-electrospray ionization-tandem mass spectrometry: method validation and application to a neonatal pharmacokinetic study. *J Chromatogr B Analyt Technol Biomed Life Sci* 1007:30–42
- Drummond IA, Davidson AJ (2010) Zebrafish kidney development. In: Detrich HW, Westerfield M, Zon LI (eds) *Methods in cell biology*. Elsevier Inc., Third Edit, pp 233–260
- Galloway CA, Yoon Y (2012) Perspectives on: SGP symposium on mitochondrial physiology and medicine: what comes first, misshape or dysfunction? The view from metabolic excess. *J Gen Physiol* 139:455–463
- Gemer O, Zaltztein E, Gorodischer R (1983) Absorption of orally administered gentamicin in infants with diarrhea. *Pediatr Pharmacol (New York)* 3:119–123
- Goldstone JV, McArthur AG, Kubota A et al (2010) Identification and developmental expression of the full complement of Cytochrome P450 genes in Zebrafish. *BMC Genomics* 11:643
- Graham GG, Scott KF (2005) Mechanism of action of paracetamol. *Am J Ther* 12:46–55
- Hentschel DM, Park KM, Cilenti L et al (2005) Acute renal failure in zebrafish: a novel system to study a complex disease. *Am J Physiol Ren Physiol* 288:F923–F929
- Herlitz LC, Mohan S, Stokes MB et al (2010) Tenofvir nephrotoxicity: acute tubular necrosis with distinctive clinical, pathological, and mitochondrial abnormalities. *Kidney Int* 78:1171–1177
- Hill A, Mesens N, Steemans M et al (2012) Comparisons between in vitro whole cell imaging and in vivo zebrafish-based approaches for identifying potential human hepatotoxicants earlier in pharmaceutical development. *Drug Metab Rev* 44:127–140
- Huang SM, Xu F, Lam SH et al (2013) Metabolomics of developing zebrafish embryos using gas chromatography- and liquid chromatography-mass spectrometry. *Mol BioSyst* 9:1372–1380

- Kersten S, Arjona FJ (2017) Ion transport in the zebrafish kidney from a human disease angle: possibilities, considerations, and future perspectives. *Am J Physiol Renal Physiol* 312:F172–F189
- Kramer-Zucker AG, Wiessner S, Jensen AM, Drummond IA (2005) Organization of the pronephric filtration apparatus in zebrafish requires nephrin, podocin and the FERM domain protein Mosaic eyes. *Dev Biol* 285:316–329
- Kremer JR, Mastrorade DN, McIntosh JR (1996) Computer visualization of three-dimensional image data using IMOD. *J Struct Biol* 116(1):71–76
- Kumai Y, Bernier NJ, Perry SF (2014) Angiotensin-II promotes Na⁺ uptake in larval zebrafish, *Danio rerio*, in acidic and ion-poor water. *J Endocrinol* 220:195–205
- Kurmi M, Golla VM, Kumar S et al (2016) Stability behaviour of antiretroviral drugs and their combinations. 4: characterization of degradation products of tenofovir alafenamide fumarate and comparison of its degradation and stability behaviour with tenofovir disoproxil fumarate. *J Pharm Biomed Anal* 131:146–155
- Levi L, Ziv T, Admon A et al (2012) Insight into molecular pathways of retinal metabolism, associated with vitellogenesis in zebrafish. *AJP Endocrinol Metab* 302:E626–E644
- Lopez-Novoa JM, Quiros Y, Vicente L et al (2011) New insights into the mechanism of aminoglycoside nephrotoxicity: an integrative point of view. *Kidney Int* 79:33–45
- Luckenbach T, Fischer S, Sturm A (2014) Current advances on ABC drug transporters in fish. *Comp Biochem Physiol Part C Toxicol Pharmacol* 165:28–52
- Mastrorade DN (1997) Dual-axis tomography: an approach with alignment methods that preserve resolution. *J Struct Biol* 120:343–352
- Mazer M, Perrone J (2008) Acetaminophen-induced nephrotoxicity: pathophysiology, clinical manifestations, and management. *J Med Toxicol* 4:2–6
- McGrath P, Li C-Q (2008) Zebrafish: a predictive model for assessing drug-induced toxicity. *Drug Discov Today* 13:394–401
- Mihaljevic I, Popovic M, Zaja R, Smital T (2016) Phylogenetic, syntenic, and tissue expression analysis of *slc22* genes in zebrafish (*Danio rerio*). *BMC Genomics* 17:626
- Nevedomskaya E, Mayboroda OA, Deelder AM (2011) Cross-platform analysis of longitudinal data in metabolomics. *Mol Biosyst* 7:3214–3222
- Olson H, Betton G, Robinson D et al (2000) Concordance of the toxicity of pharmaceuticals in humans and in animals. *Regul Toxicol Pharmacol* 32:56–67
- Pacchiarotta T, Hensbergen PJ, Wuhrer M et al (2012) Fibrinogen alpha chain *O*-glycopeptides as possible markers of urinary tract infection. *J Proteomics* 75:1067–1073
- Pannicke U, Hönig M, Hess I et al (2009) Reticular dysgenesis (aleukocytosis) is caused by mutations in the gene encoding mitochondrial adenylate kinase 2. *Nat Genet* 41:101–105
- Peng H-C, Wang Y-H, Wen C-C et al (2010) Nephrotoxicity assessments of acetaminophen during zebrafish embryogenesis. *Comp Biochem Physiol C Toxicol Pharmacol* 151:480–486
- Peterson RT, MacRae CA (2012) Systematic approaches to toxicology in the zebrafish. *Annu Rev Pharmacol Toxicol* 52:433–453
- Pluskal T, Castillo S, Villar-Briones A, Oresic M (2010) MZmine 2: modular framework for processing, visualizing, and analyzing mass spectrometry-based molecular profile data. *BMC Bioinformatics* 11:395
- Price VR (2002) ATP depletion of tubular cells causes dissociation of the zonula adherens and nuclear translocation of—catenin and LEF-1. *J Am Soc Nephrol* 13:1152–1161
- Rafelski SM (2013) Mitochondrial network morphology: building an integrative, geometrical view. *BMC Biol* 11:71
- Randhawa MA (2009) Calculation of LD50 values from the method of Miller and Tainter, 1944. *J Ayub Med Coll Abbottabad* 21:184–185
- Rider SA, Tucker CS, Del-Pozo J et al (2012) Techniques for the in vivo assessment of cardio-renal function in zebrafish (*Danio rerio*) larvae. *J Physiol* 590:1803–1809
- Rider SA, Mullins LJ, Verdon RF et al (2015) Renin expression in developing zebrafish is associated with angiogenesis and requires the notch pathway and endothelium. *Am J Physiol Ren Physiol* 309:F531–F539
- Saad M, Cavanaugh K, Verbueken E et al (2016) Xenobiotic metabolism in the zebrafish: a review of the spatiotemporal distribution, modulation and activity of Cytochrome P450 families 1 to 3. *J Toxicol Sci* 41:1–11
- Schieber NL, Nixon SJ, Webb RI et al (2010) Modern approaches for ultrastructural analysis of the zebrafish embryo. *Methods Cell Biol* 96:425–442
- Schindelin J, Arganda-Carreras I, Frise E et al (2012) Fiji: an open-source platform for biological-image analysis. *Nat Methods* 9:676–682
- Schindelin J, Rueden CT, Hiner MC, Eliceiri KW (2015) The ImageJ ecosystem: an open platform for biomedical image analysis. *Mol Reprod Dev* 82:518–529
- Smith KY, Patel P, Fine D et al (2009) Randomized, double-blind, placebo-matched, multicenter trial of abacavir/lamivudine or tenofovir/emtricitabine with lopinavir/ritonavir for initial HIV treatment. *AIDS* 23:1547–1556
- Tourret J, Deray G, Isnard-Bagnis C (2013) Tenofovir effect on the kidneys of HIV-infected patients: a double-edged sword? *J Am Soc Nephrol* 24:1519–1527
- Westhoff JH, Giselbrecht S, Schmidts M et al (2013) Development of an automated imaging pipeline for the analysis of the zebrafish larval kidney. *PLoS ONE* 8:1–13
- Wingert RA, Davidson AJ (2008) The zebrafish pronephros: a model to study nephron segmentation. *Kidney Int* 73(10):1120–1127
- Wingert RA, Selleck R, Yu J et al (2007) The *cdx* genes and retinoic acid control the positioning and segmentation of the zebrafish pronephros. *PLoS Genet* 3:1922–1938
- Youle RJ, van der Bliek AM (2012) Mitochondrial fission, fusion, and stress. *Science* 337:1062–1065